Guided plasmonic modes of anisotropic slot waveguides

2012 Nanotechnology 23 444006

(http://iopscience.iop.org/0957-4484/23/44/444006)

Nanotechnology **23** (2012) 444006 (8pp) doi:10.1088/0957-4484/23/44/444006

Guided plasmonic modes of anisotropic slot waveguides

Ivan D Rukhlenko[1], **Malin Premaratne**[1] **and Govind P Agrawal**[2]

[1] Advanced Computing and Simulation Laboratory, Monash University, Clayton, Victoria 3800, Australia
[2] The Institute of Optics, University of Rochester, Rochester, NY 14627, USA

E-mail: ivan.rukhlenko@monash.edu

Received 11 February 2012, in final form 9 April 2012
Published 18 October 2012
Online at stacks.iop.org/Nano/23/444006

Abstract
We study guided optical modes of a planar plasmonic waveguide filled with a generic anisotropic medium. In particular, we show that both surface and oscillatory modes exist for such waveguides and find their numbers for two specific forms of the anisotropy tensor. We also show that lossless waveguides, characterized by a diagonal permittivity tensor, support simultaneously both the forward and backward propagating modes (surface or oscillatory type) with antisymmetric field patterns. Another family of guided oscillatory modes may be supported by the waveguide if its anisotropy is created by an external magnetic field. These new modes are asymmetric in nature, exhibit extremely low effective refractive indices and may propagate over macroscopic distances without significant attenuation, while remaining strongly confined to the waveguide.

(Some figures may appear in colour only in the online journal)

1. Introduction

The vast amount of traffic supported by optical fibers allows communications of unprecedented speed and quality, limited solely by hardware performance. It is anticipated that the operating speed of hardware may be enhanced—to match the network capacity—by replacing electronic circuits with all-optical photonic chips and using light for data processing. Unfortunately, infrared light itself cannot be confined to areas smaller than the half of its wavelength (∼500 nm), and hence it is unable to provide the extent of miniaturization achievable with nanoelectronics (∼50 nm) [1]. This problem may be solved by coupling infrared light to conduction electrons localized in the vicinity of metal–dielectric interfaces, and handling information in the form of surface plasmons [2–5]. The performance of a photonic circuit embodying this concept greatly relies on the efficiency of the surface-plasmon guidance, a topic studied extensively over the past decade [6–10].

Among the well-explored geometries supporting surface plasmons are circular nanowires [11–17], one-dimensional chains of metallic nanospheres [18–23], and planar metal–dielectric–metal waveguides [24–27] made of isotropic and homogeneous media. One of the features found to be common for all three structures is that their characteristic lateral dimensions (radii for nanowires and nanospheres and dielectric gap thickness for planar waveguides) determine the balance between the guiding and confining efficiencies: the smaller these dimensions, the higher the confinement and the stronger the absorption losses. Despite substantial research efforts devoted to the study of surface plasmons under various conditions, there are still many issues that remain to be clarified and merit further consideration. As a vivid illustration of this point, we refer to the recent papers of Feigenbaum *et al* [28] and Davoyan *et al* [29], in which the authors revealed the existence of an additional, backward mode guided by linear slot waveguides. The surprising thing is that this mode had gone unnoticed for nearly 20 years since the profound theoretical study conducted by Prade *et al* [30].

With the recent progress in fabrication of advanced nanostructured composites, experimentalists and engineers increasingly find themselves facing a lack of sufficient theoretical descriptions of various metamaterial structures, even though their analogs made of naturally occurring media are well understood based on a solid theoretical framework. The models developed for ordinary structures are

usually inapplicable to metamaterials due to the pronounced anisotropy of their electromagnetic properties [31]. The metal–dielectric structures are no exception and require re-examination when anisotropy is present.

In this paper we present the first theoretical study of planar, plasmonic, slot waveguides filled with a generic anisotropic material. Specifically, we analyze both the surface and oscillatory guided modes in the case of an anisotropic dielectric slab made of an orthorhombic crystal, and determine the parameter values for which they propagate forward or backward. Our results generalize as well as extend the results of [29, 30]. Owing to the existence of backward propagating modes, characterized by opposite directions of the phase and group velocities, metal–dielectric–metal (MDM) structures find use in subwavelength optical imaging [32–34]. We also reveal a new family of quasi-static oscillatory modes that arise in the event that the anisotropy is created by an external magnetic field. These modes exhibit extremely low effective refractive indices and may propagate over macroscopic distances without significant attenuation, while remaining strongly confined to the waveguide.

2. Maxwell's equations and surface-plasmon modes

Figure 1 shows the planar waveguide analyzed in this paper. It consists of an anisotropic, nonmagnetic, dielectric slab of thickness $2h$ surrounded by metal claddings of permittivity $\varepsilon_{\rm m} = \varepsilon'_{\rm m} + {\rm i}\varepsilon''_{\rm m}$. We suppose that the slab's permittivity is described by a constant tensor of the form

$$\hat{\epsilon} = \begin{pmatrix} \varepsilon_{xx} & 0 & \varepsilon_{xz} \\ 0 & \varepsilon_{yy} & 0 \\ \varepsilon_{zx} & 0 & \varepsilon_{zz} \end{pmatrix}, \qquad (1)$$

which may account for the anisotropy that is intrinsic to the slab or induced by external fields. In the geometry used for figure 1, only the transverse-magnetic (TM) modes preserve their initial states of polarization during their propagation in the z direction. We restrict our consideration to these modes and assume that the slab is nonabsorbing, in which case its permittivity tensor is Hermitian, $\epsilon^*_{ik} = \epsilon_{ki}$ [35].

We represent the electric and magnetic fields of a monochromatic TM mode as

$$\mathbf{E}(x, z, \omega) = (\hat{x}E_x + {\rm i}\hat{z}E_z)\, {\rm e}^{{\rm i}\beta(\omega)z} + {\rm c.c.},$$
$$\mathbf{H}(x, z, \omega) = \hat{y}H_y\, {\rm e}^{{\rm i}\beta(\omega)z} + {\rm c.c.},$$

where $\hat{s}$ is the unit vector along the s axis, $\beta(\omega) = \beta' + {\rm i}\beta''$ is the propagation constant, and ω is the mode's frequency. Inside the slab ($|x| < h$), Maxwell's equations reduce to the following two equations for the electric field components:

$$\frac{\partial E_x}{\partial x} = 2\eta E_x + aE_z, \qquad (2)$$

$$\frac{\partial E_z}{\partial x} = (\beta - \varepsilon_{xx}\vartheta k)\, E_x - {\rm i}\varepsilon_{xz}\vartheta k E_z, \qquad (3)$$

where $\eta = ({\rm i}/2)[\varepsilon_{xz}\vartheta k - (\varepsilon_{xz} + \varepsilon_{zx})\beta/\varepsilon_{xx}]$, $\vartheta = k/\beta$, $a = (\varepsilon_{zz}\beta - \varepsilon^2_{xz}\vartheta k)/\varepsilon_{xx}$, $k = \omega/c$, and c is the speed of light in a vacuum.

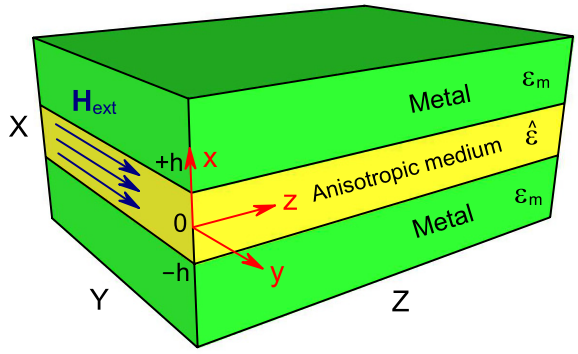

Figure 1. Metal–dielectric–metal slot waveguide of thickness $2h$ filled with an anisotropic medium. The waveguide edges are aligned with the coordinate axes.

Equations (2) and (3) can be solved easily owing to their linear nature, and their general solution can be written in the form

$$E_x = [(aA_1 + \eta A_2)\sinh(qx) + qA_2\cosh(qx)]\, {\rm e}^{\eta x}, \qquad (4a)$$
$$E_z = [(bA_2 - \eta A_1)\sinh(qx) + qA_1\cosh(qx)]\, {\rm e}^{\eta x}, \qquad (4b)$$

where $b = \beta - (\varepsilon_{xx} + {\rm i}\varepsilon_{xz})\vartheta k$, $q = \sqrt{ab + \eta^2}$, and A_1 and A_2 are the integration constants. The electric field of a guided mode confined to the slab should evanescently decay inside the metal regions $|x| > h$. Thus, we can write it in the form $E^{\pm}_x = B_{\pm}{\rm e}^{k_{\rm m}(h\mp x)}$, with $k_{\rm m} = \sqrt{\beta^2 - \varepsilon_{\rm m}k^2}$ and $B_{\pm}$ being constants. Here, the $\pm$ signs of the component $E^{\pm}_x$ correspond to regions $x > h$ and $x < -h$, respectively.

Using the standard boundary conditions at $x = \pm h$ interfaces, we obtain the dispersion relation for guided TM modes in the form

$$\varepsilon_{\rm m}q = \tanh(2qh)\left({\rm i}\varepsilon_{xz}\eta\chi - \frac{\varepsilon_{xx}}{2}(\chi a + \psi b)\right), \qquad (5)$$

where $\chi = k_{\rm m}/\beta$ and $\psi = [\varepsilon^2_{\rm m} + (\varepsilon_{xz}\chi)^2]/(\varepsilon^2_{xx}\chi)$. By choosing $B_+ = 1$, the coefficients A_1, A_2, and B_- are given by

$$A_1 = -\left[b\tau S + (qC + \eta S)\chi\right]/q^2,$$
$$A_2 = \left[a\chi S + (qC - \eta S)\tau\right]/q^2,$$
$$B_- = -\left[(aS + 2q\tau C/\chi)bS + (qC + \eta S)^2\right]{\rm e}^{-2\eta h}/q^2,$$

where $S = \sinh(qh)$, $C = \cosh(qh)$, and $\tau = (\varepsilon_{\rm m} + {\rm i}\chi\varepsilon_{xz})/\varepsilon_{xx}$. The magnetic field of the guided mode is related to the electric field as $H_y = (\varepsilon_0\omega/\beta)(\varepsilon_{xx}E_x + {\rm i}\varepsilon_{xz}E_z)$.

3. Guided modes for a diagonal permittivity tensor

The presence of the exponential factor in equation (4) indicates that an anisotropic plasmonic waveguide does not generally support guided modes of a definite symmetry. These modes may be divided into symmetric (s) and antisymmetric (a) types only when the off-diagonal elements vanish, i.e. $\varepsilon_{xz} = \varepsilon_{zx} = 0$. This can occur for uniaxial and biaxial crystals whose crystallographic axes coincide with the waveguide edges, as well as for isotropic crystals exposed to

an external electric field parallel to one of the waveguide's edges. For example, an electrostatic field $\mathbf{E}_{\rm ext} = \hat{x}E_0$ ($E_0 \gg |E_x|$) applied to an isotropic slab with $\hat{\varepsilon} = \varepsilon\delta_{ik}$, alters the slab's permittivity in the direction parallel to the field, $\varepsilon_{xx} = \varepsilon + \alpha E_0^2$, but does not change the permittivities in the y and z directions ($\varepsilon_{yy} = \varepsilon_{zz} = \varepsilon$).

When the off-diagonal components of the permittivity tensor are set to zero, equation (5) reduces to two dispersion relations of the form

$$\tanh(qh) = -\left(\frac{k_{\rm m}}{q}\frac{\varepsilon_{zz}}{\varepsilon_{\rm m}}\right)^{\pm 1}, \tag{6}$$

where $q = \sqrt{(\varepsilon_{zz}/\varepsilon_{xx})\beta^2 - \varepsilon_{zz}k^2}$ and the $\pm$ signs correspond to the symmetric and antisymmetric modes, respectively; the symmetric (antisymmetric) mode is characterized by even (odd) functions $E_x(x)$ and $H_y(x)$.

Similar to the isotropic case, anisotropic MDM waveguides described by equation (6) support both the surface and oscillatory guided modes [30]. The existence and properties of these modes can be easily analyzed for zero losses ($\varepsilon_{\rm m}'' = 0$). In this case, the two mode families are described by a purely real or a purely imaginary value of q.

3.1. Surface modes

Following [30], we introduce the new parameters $u = h\sqrt{\beta^2 - \varepsilon_{xx}k^2}$, $v = kh\sqrt{\varepsilon_{xx} - \varepsilon_{\rm m}}$, and $w = u/v$ and use them to rewrite the dispersion relations in equation (6) as

$$v(w) = \frac{\sqrt{\sigma}}{2w}\ln\left(\pm\frac{\sqrt{\rho}w + \sqrt{w^2+1}}{\sqrt{\rho}w - \sqrt{w^2+1}}\right), \tag{7}$$

where $\rho = r_x r_z$, $\sigma = r_z/r_x$, and $r_j = -\varepsilon_{\rm m}/\varepsilon_{jj} > 0$ ($j = x, z$). According to this expression, the number of surface modes in the entire range of kh does not depend on σ. Noting that the parameters v and w are positive ($0 \le w < \infty$) and that the propagation constant can be found by calculating the inverse function $w(v)$, one can draw the following conclusions. If $\rho \le 1$ (i.e. $\varepsilon_{\rm m}^2 \le \varepsilon_{xx}\varepsilon_{zz}$), then the waveguide supports only one backward antisymmetric mode with the cutoff (see appendix A)

$$(kh)_{\rm sup} = \frac{r_z}{\sqrt{\varepsilon_{xx} - \varepsilon_{\rm m}}}. \tag{8}$$

For $\rho > 1$ ($\varepsilon_{\rm m}^2 > \varepsilon_{xx}\varepsilon_{zz}$) one symmetric mode without a cutoff and either one or two antisymmetric modes with a lower cutoff $(kh)_{\rm inf}$ exist. Some algebra shows (see appendix B) that for $\rho \ge 3/2$ there is only one mode of each symmetry characterized by a positive group velocity. For $1 < \rho < 3/2$ two antisymmetric modes of the same frequency coexist in the range $(kh)_{\rm inf} < kh < (kh)_{\rm sup}$, where $(kh)_{\rm sup}$ is given in equation (8). One of the modes (with larger β) propagates forward and the other (with smaller β) backward. These modes represent the two parts of the dispersion branch $\omega_{\rm a}(\beta)$ separated by a minimum point where the average power flow vanishes [29]. For $\rho \ge 3/2$, the cutoff $(kh)_{\rm inf}$ of the antisymmetric mode coincides with $(kh)_{\rm sup}$ in equation (8). Figure 2 illustrates the above discussion. Note also that, in practice, $\rho \gg 1$ since $-\varepsilon_{\rm m}'$ for most metals is much larger than both ε_{xx} and ε_{zz}.

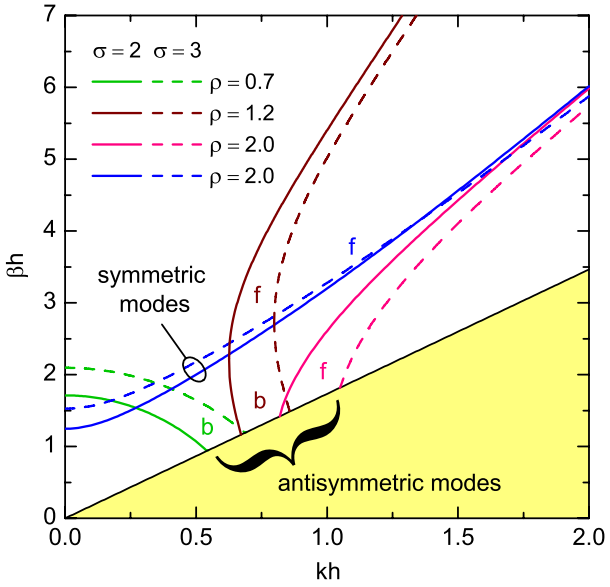

Figure 2. Dispersion curves for surface-plasmon modes of an anisotropic slot waveguide (in the absence of absorption) for two values of σ and four values of ρ with $\varepsilon_{xx} = 3$ in all cases. Forward and backward modes are marked as f and b; the shaded area marks the region $\beta < k\sqrt{\varepsilon_{xx}}$.

3.2. Oscillatory modes

In contrast to a maximum of three surface modes that may be supported by an anisotropic slot waveguide, a much larger number of oscillatory modes may be guided if the plasmonic waveguide is sufficiently thick. The existence of these modes, with $u = h\sqrt{\varepsilon_{xx}k^2 - \beta^2} > 0$, is analyzed in a similar fashion. Equation (6) for such modes is of the form

$$v(w) = \frac{\sqrt{\sigma}}{w}\left[\pi n \mp \tan^{-1}\left(\frac{1-w^2}{\rho w^2}\right)^{\pm 1/2}\right], \tag{9}$$

where $0 \le w < (1 + r_x)^{-1/2}$, n is an integer, and the upper (lower) sign corresponds to the symmetric (antisymmetric) mode. It is seen that the number of oscillatory modes depends drastically on the parameters kh, r_x, and r_z. Specifically, the lowest-order antisymmetric mode (with $n = 0$) exists in the range

$$\min(\zeta_1, \zeta_2) < kh < \max(\zeta_1, \zeta_3), \tag{10}$$

where $\zeta_1 = \varepsilon_{zz}^{-1/2}\tan^{-1}\sqrt{r_z}$, $\zeta_2 = v(w_{\rm m})/\sqrt{\varepsilon_{xx} - \varepsilon_{\rm m}}$, $\zeta_3 = r_z/\sqrt{\varepsilon_{xx} - \varepsilon_{\rm m}}$, and $w_{\rm m} > 0$ is the minimum of the function $v(w)$. The rest of the modes exhibit a lower cutoff given by the expression

$$(kh)_{\rm inf} = \frac{1}{\sqrt{\varepsilon_{zz}}}\left(\pi n \mp \tan^{-1}(r_z)^{\mp 1/2}\right), \tag{11}$$

in which, as before, the upper and lower signs correspond to the symmetric and antisymmetric modes, respectively. Equations (10) and (11) show that the waveguide does not

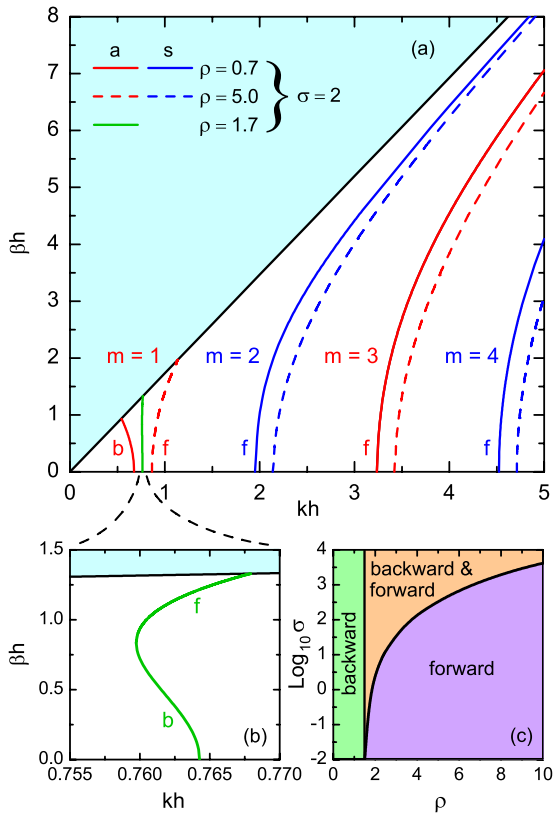

Figure 3. (a) Dispersion curves for oscillatory plasmon modes of an anisotropic slot waveguide in the absence of absorption using $\varepsilon_{xx} = 3$. Forward and backward modes are marked as *f* and *b*; the shaded area marks the region $\beta > k\sqrt{\varepsilon_{xx}}$. (b) Magnified dispersion curve for the ($m = 1$) antisymmetric mode and (c) its propagation regimes in the ρ–σ plane.

support oscillatory modes if $kh < (kh)_{\min} = \min(\zeta_1, \zeta_2)$. In a typical case of $\varepsilon_{zz} \ll -\varepsilon_{\rm m}$, this condition gives $(kh)_{\min} = \zeta_1$. The mode $n = 0$ then exists for

$$\varepsilon_{zz}^{-1/2} \tan^{-1}\sqrt{r_z} < kh < r_z/\sqrt{\varepsilon_{xx} - \varepsilon_{\rm m}}. \tag{12}$$

It is convenient to number the oscillatory modes consecutively using integers $m = 1, 2, 3, \ldots$, so that the mode's parity coincides with the parity of the mode number m. This indexing scheme is established by representing the expression in the parenthesis of equation (11) in the form $\frac{\pi}{2}(m-1) + \tan^{-1}\sqrt{r_z}$. The dispersion curves of the first four oscillatory modes are shown in figure 3(a).

The structure of the mode with $m = 1$ is controlled by the parameters ρ and σ, and it deserves special consideration. It is not hard to show (see appendix C) that this mode propagates backward for $\rho < 3/2$ regardless of σ. For $3/2 \le \rho < \rho_{\rm r}(\sigma)$, where $\rho_{\rm r}(\sigma)$ is the root of equation (C.3), this mode consists of the forward and backward branches shown in figure 3(b). The mode is forward for $\rho > \rho_{\rm r}(\sigma)$. Figure 3(c) shows all three states of the described mode in the ρ–σ plane. While the possibility of the simultaneous existence of forward and backward surface modes in isotropic MDM waveguides—initially overlooked by Prade and co-workers [30]—was recently revealed by Feigenbaum *et al* [28] and Davoyan *et al* [29], the same feature for the oscillatory modes has never been reported until now.

4. Oscillatory modes for magneto-optical anisotropy

In this section we focus on the case in which all off-diagonal elements of the permittivity tensor in equation (1) do not vanish. An important case is the one in which $\varepsilon_{xx} = \varepsilon_{yy} = \varepsilon_{zz} = \varepsilon$ and $\varepsilon_{xz} = \varepsilon_{zx}^{*} = -{\rm i}\gamma$. It describes the situation where an isotropic material is exposed to an external magnetic field parallel to the y axis ($\mathbf{H}_{\rm ext} = \hat{y}H_0$). In this specific case, the value of the parameter γ is determined by the field amplitude H_0 (which should be much stronger than the magnetic field H_y of the plasmon mode), and the generalized symmetry principle for kinetic coefficients requires γ to change its sign upon reversing the direction of $\mathbf{H}_{\rm ext}$ [35].

The general analysis of equation (5) in the case of magneto-optical anisotropy is quite complicated, except when the magnetic field is relatively weak and the parameters ε, γ, and $\varepsilon_{\rm m}$ are restricted to their 'ordinary' values in the optical range ($\varepsilon > 1$, $\gamma \ll \varepsilon$, and $\varepsilon_{\rm m}'' \ll -\varepsilon_{\rm m}'$). Then, in addition to the modes that in the isotropic limit reduce to those following from equation (6), a countable set of strongly asymmetric oscillatory modes arises when a magnetic field is applied. These modes stem from the guided modes of the lossless waveguide and satisfy the following approximate dispersion relation:

$$\varphi\gamma k \tan(2\xi\gamma k^2 h/\beta) \approx 2\xi\beta\sqrt{-\varepsilon_{\rm m}}, \tag{13}$$

in which $\varphi = 1 + \gamma/\varepsilon$ and $\xi = \sqrt{3/4 + \gamma/\varepsilon}$. In deriving this expression from equation (5), we have assumed that $|\beta| \ll \gamma k$ and $\gamma < 1$. Since these inequalities lead to $k_{\rm m}^2 \approx -\varepsilon_{\rm m} k^2$, the skin depth δ of these modes is nearly independent of the propagation constant (and waveguide thickness) and is given by $\delta \approx k^{-1}(-\varepsilon_{\rm m}')^{-1/2}$. As we shall see later, the employed approximation is well justified by the final solution.

In sharp contrast to the ordinary oscillatory modes found earlier, the new asymmetric modes always propagate forward, do not exhibit a cutoff, and exist regardless of the dielectric slab thickness. This follows from equation (13), which has real solutions for any real values of the waveguide parameters, provided that $\varepsilon_{\rm m} < 0$. In the limit $h \to 0$, this equation is readily solved to yield

$$\beta \approx \frac{\gamma k}{4\xi\sqrt{-\varepsilon_{\rm m}}}\left(\sqrt{(4\xi)^2\varphi kh\sqrt{-\varepsilon_{\rm m}} + [\pi(n-1)\varphi]^2} - \pi(n-1)\varphi\right). \tag{14}$$

This result shows that the propagation length,

$$L_{\rm SPP} = \left(\frac{-\varepsilon_{\rm m}'}{\pi\varepsilon_{\rm m}''}\right)\lambda_{\rm eff}, \tag{15}$$

of the fundamental plasmon mode ($n = 1$) varies in proportion to the effective wavelength

$$\lambda_{\rm eff} = \frac{\lambda}{\gamma}\left(\frac{\sqrt{-\varepsilon_{\rm m}'}}{\varphi kh}\right)^{1/2} \tag{16}$$

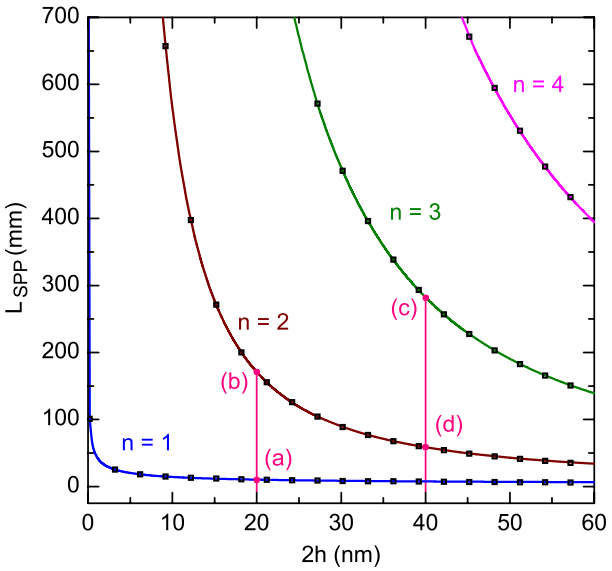

Figure 4. Propagation length as a function of waveguide thickness for the first four asymmetric oscillatory modes using $\gamma = 0.01$. Solid curves represent the exact solution of equation (5), while square symbols show the approximate solution in equation (14). Electric and magnetic field profiles for points (a)–(d) are shown in figure 5. For simulation parameters, refer to the text.

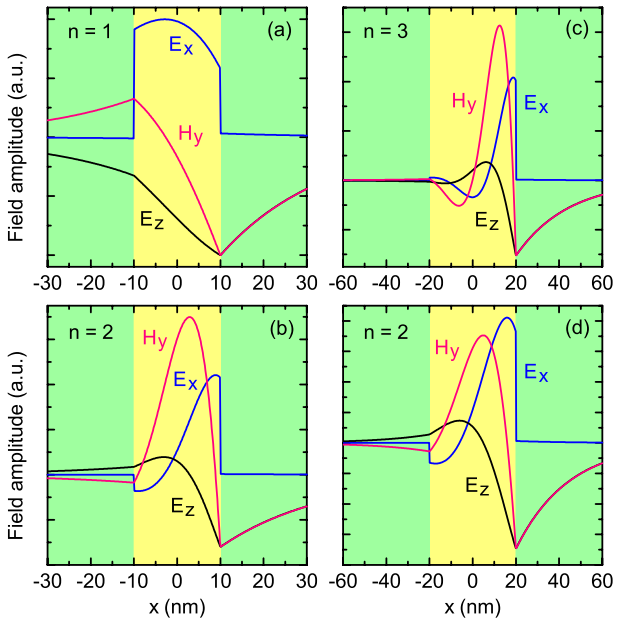

Figure 5. Electric and magnetic field profiles for the first three asymmetric oscillatory modes in the cases of 20 and 40 nm thick waveguides. The four panels correspond to the four points marked by red vertical lines in figure 4.

of this mode, for a fixed $\lambda = 2\pi/k$. It is seen that both λ_{eff} and L_{SPP} diverge as h approaches zero. They also diverge for $\gamma \to 0$, but with a proportionality factor different from that in equation (16). Since β decreases with n in the absence of metallic losses, the effective wavelength and propagation length of the modes with $n > 1$ also diverge in the above two limits. In most practical situations $\gamma \ll \varepsilon$, and the magneto-optical anisotropy only slightly perturbs the symmetry of the standard SPP modes following from equation (6).

To illustrate the preceding results with an example, we fix the free-space wavelength $\lambda = 1.55\ \mu$m and focus on a MDM waveguide made of a dielectric with $\varepsilon = 3$ and $\gamma = 0.01$ and sandwiched between two silver layers with permittivity $\varepsilon_{\text{m}}(\lambda) = -104.3 + 8.1\text{i}$ [25]. Figure 4 shows the propagation length L_{SPP} of the four oscillatory modes supported by this waveguide. The first extraordinary feature of these modes is their almost lossless propagation over macroscopic distances of tens or hundreds of millimeters. The effective wavelengths of these modes are much larger than λ, as is evidenced by the example of the lowest-order mode for which equation (15) gives $L_{\text{SPP}} \approx 4\lambda_{\text{eff}}$. The ratio between L_{SPP} and λ_{eff} grows with increasing mode number, and for large values of n it is given by the expression

$$\frac{L_{\text{SPP}}}{\lambda_{\text{eff}}} \approx \frac{\pi\varphi}{8\xi^2 kh}\frac{\sqrt{-\varepsilon'_{\text{m}}}}{\varepsilon''_{\text{m}}}(n-1)^2,$$

while the effective wavelength is given by

$$\lambda_{\text{eff}} \approx \frac{\pi(n-1)}{2\gamma\xi kh}\lambda.$$

Note that the substantial propagation distances shown in figure 4 and large values of λ_{eff} do not prevent transverse localization of the oscillatory modes on a subwavelength scale, determined by the parameter $\delta \approx 24$ nm. It is also important that the number of asymmetric modes supported by a given waveguide is independent of the waveguide thickness. These features set the newly discovered family of guided modes far apart from the oscillatory modes of definite symmetry, which according to equation (12) are not supported by waveguides of thicknesses less than 400 nm (for the same material parameters). Clearly, these new types of oscillatory modes should prove quite useful for efficient guidance of optical energy on the nanoscale.

Figure 5 shows the mode profiles calculated for the four modes corresponding to the points (a)–(d) in figure 4; its left and right columns correspond to MDM waveguides that are 20 and 40 nm thick, respectively. One can see that the modes are predominantly localized in the vicinity of one of the metal–dielectric interfaces, with the mode number n corresponding to the number of sign changes of the magnetic field within the dielectric slab. The electric field component $\hat{x}E_x$ is about two orders of magnitude smaller than $\hat{z}E_z$ in all four cases, and has opposite directions in the two metallic cladding layers.

5. Conclusions

We have analyzed the existence of guided TM modes in MDM-type plasmonic waveguides whose thin dielectric layer consists of an anisotropic material. It was found that both surface and oscillatory modes exist for such waveguides but their number depends on the specific form of the anisotropy tensor associated with the central dielectric layer. Lossless waveguides, characterized by a diagonal permittivity tensor, support simultaneously both the forward

and backward propagating modes (surface or oscillatory type) with antisymmetric field patterns.

We also analyzed the case of a non-diagonal permittivity tensor in the situation in which the central dielectric layer of the MDM waveguide consists of an isotropic material, but it becomes anisotropic when an external magnetic field is applied along the lateral direction perpendicular to the direction of wave propagation. In this situation, we have found that the waveguide supports a new family of asymmetric oscillatory modes that are characterized by a relatively low effective refractive index that depends on the strength of the magnetic field. The most interesting, and practically useful, property of these modes is that they can propagate over macroscopic distances (>1 cm) without significant attenuation, while remaining strongly confined to the slot waveguide of subwavelength thickness (<100 nm). We emphasize that such antisymmetric oscillatory modes are characterized by relatively long wavelengths ($|\beta|/k \ll 1$), which makes their propagation essentially quasi-static and analogous to that occurring in a metamaterial exhibiting a refractive index of nearly zero. The experimental study of these modes can therefore be used to prototype the optical behavior of such metamaterials with an index near zero.

Acknowledgments

This work was supported by the Australian Research Council through its Discovery Grant scheme under grant DP110100713 and through its Discovery Early Career Researcher Award DE120100055.

Appendix A

To understand the behavior of the antisymmetric surface mode with changing parameter $\rho < 1$, we first calculate the derivative of the function $v(w)$ given in equation (7):

$$v'(w) = \frac{v\left[1-(\rho-1)\,w^2\right]\sqrt{1+w^2}-\sqrt{\rho\sigma}}{w\left[1-(\rho-1)\,w^2\right]\sqrt{1+w^2}}. \quad \text{(A.1)}$$

This derivative is related to the tilt of the dispersion curve:

$$\frac{\partial k}{\partial \beta} = \frac{(k/\beta)v'}{v' + v^3 w/(\beta h)^2}, \quad \text{(A.2)}$$

where we assumed the permittivities to be constant and thus neglected material dispersion.

For small values of w, we can approximate v as $v \approx \sqrt{\rho\sigma}$. In the same limit

$$v' \approx \sqrt{\rho\sigma}\left(\frac{2}{3}\,\rho - 1\right) w$$

and

$$\beta h \approx \frac{r_z}{\sqrt{1+r_x}}.$$

Using these results in equation (A.2), we obtain

$$\lim_{w\to 0}\frac{\partial k}{\partial \beta} \approx \frac{(2\rho-3)\vartheta}{2\rho + 3\sqrt{\rho/\sigma}}. \quad \text{(A.3)}$$

In the opposite limit $w \to \infty$, we can employ the approximations

$$v \approx \frac{\sqrt{\sigma}}{2w}\ln\frac{1+\sqrt{\rho}}{1-\sqrt{\rho}},$$

$$v' \approx -\frac{\sqrt{\sigma}}{2w^2}\ln\frac{1+\sqrt{\rho}}{1-\sqrt{\rho}} - \frac{3\sqrt{\rho\sigma}}{2(\rho-1)w^4},$$

and $\beta h \approx \sqrt{\sigma}\tanh^{-1}\sqrt{\rho}$. Using them in equation (A.2), we obtain

$$\left.\frac{\partial k}{\partial \beta}\right|_{w\to\infty} \sim \frac{2(\rho-1)w^2 kh}{3\sqrt{\rho\sigma}}. \quad \text{(A.4)}$$

Since the derivative $v'(w)$ cannot change its sign for positive w more than once (see appendix B), equations (A.3) and (A.4) suggest that $\partial k/\partial\beta < 0$ for $\rho < 1$ regardless of σ, i.e. the antisymmetric surface mode is propagating backwards.

Appendix B

Consider next the antisymmetric surface mode for $\rho > 1$. Since $v(w)$ for this mode is even, the derivative $v'(0) = 0$, and the extrema of $v(w)$ can be found by setting the numerator of equation (A.1) to zero. This yields the following cubic equation with respect to the unknown $W = w^2$:

$$(\rho-1)^2 W^3 + (\rho-3)\,(\rho-1)\,W^2 + (3-2\rho)\,W + 1 - \rho\sigma/v^2 = 0.$$

The three roots of this equation depend on the specific values of ρ, v, and σ. Only real roots are physically meaningful. For small values of w, $v^2 = \rho\sigma$, and one of the roots of the cubic polynomial must vanish, say $W_1 = 0$. The remaining two roots are either complex or both real. In the second case, only the positive root, say $W_2 = w_{\rm m}^2 > 0$, is physically meaningful (see figure B.1).

Since $v \to \infty$ as w approaches $(\rho-1)^{-1/2}$, the function $v(w)$ either grows monotonously for all w or decreases for $w < w_{\rm m}$ and then grows for $w > w_{\rm m}$. By expanding $v'(w)$ in Taylor series

$$v'(w) = \sqrt{\rho\sigma}\left(\tfrac{2}{3}\,\rho - 1\right) w + \sqrt{\rho\sigma}\left(\tfrac{4}{5}\,\rho^2 - 2\rho + \tfrac{3}{2}\right) w^3 + O(w^5),$$

we see that the first situation is realized when $\rho \geq 3/2$, while the second occurs for $\rho < 3/2$. In the first case, only one mode with a lower cutoff, determined by the condition $v = v(0) = \sqrt{\rho\sigma}$, exists. Equation (A.3) and the limit

$$\lim_{w\to\infty}\frac{\partial k}{\partial \beta} = \frac{\sqrt{\rho\sigma}+1}{(-\varepsilon_{\rm m})(\rho-1)} > 0 \quad \text{(B.1)}$$

indicate that this mode is forward propagating. Analogously, we conclude that in the second case two modes (forward and backward) coexist for $v(w_{\rm m}) < v < v(0)$, and one forward mode exists for $v > v(0)$.

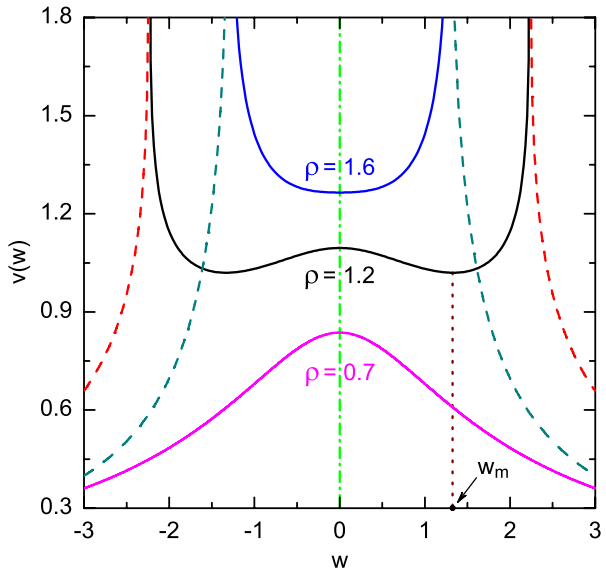

Figure B.1. Function $v(w)$ for symmetric (dashed curves) and antisymmetric (solid curves) guided plasmon modes of anisotropic slot waveguides characterized by three values of ρ and $\sigma = 1$. Only positive values of w are physically meaningful.

Appendix C

According to equation (9), the derivative of the function $v(w)$ for the antisymmetric oscillatory mode $m = 1$ is

$$v'(w) = \frac{\sqrt{\rho\sigma} - v[1 + (\rho - 1)w^2]\sqrt{1 - w^2}}{w[1 + (\rho - 1)w^2]\sqrt{1 - w^2}}.$$

The expression for $\partial k/\partial\beta$ differs from that in equation (A.2) by only a sign and is given by

$$\frac{\partial k}{\partial \beta} = -\frac{(k/\beta)v'}{v' + v^3 w/(\beta h)^2}. \tag{C.1}$$

Unlike the antisymmetric surface mode considered before, now $v(w)$ does not diverge, and the parameter w is bounded above by the value $w_{\max} = (1 + r_x)^{-1/2}$. This results in the following three possibilities: (i) the function v grows monotonously for all w; (ii) v decreases for $w < w_{\rm m} < w_{\max}$ and grows for $w > w_{\rm m}$, where $w_{\rm m}$ is the nonzero root of the equation $v'(w) = 0$; and (iii) v decreases monotonously for all w. By expanding $v'(w)$ in a Taylor series

$$v'(w) = \sqrt{\rho\sigma}\left(1 - \frac{2}{3}\rho\right)w + \sqrt{\rho\sigma}\left(\frac{4}{5}\rho^2 - 2\rho + \frac{3}{2}\right)w^3 + \mathrm{O}(w^5),$$

we conclude that the first possibility is realized for $\rho < 3/2$, whereas the last two occur for $\rho \geq 3/2$. In the limit $w \to w_{\max}$ ($\beta \to 0$), the tilt of the dispersion curve approaches zero as

$$\frac{\partial k}{\partial \beta} \sim \frac{r_x(1 + r_z)\tan^{-1}\sqrt{r_z} - (1 + r_x)\sqrt{r_z}}{\sigma r_x(1 + r_z)\sqrt{1 + r_x}\left(\tan^{-1}\sqrt{r_z}\right)^3}\beta k h^2. \tag{C.2}$$

This result, together with equations (C.1) and (A.3), shows that the above three possibilities correspond to a single backward mode, one forward mode and one backward mode, and a single forward mode, respectively. The second and third regimes change each other when ρ and σ (or r_x and r_z) are such that

$$(1 + r_x)\sqrt{r_z} = r_x(1 + r_z)\tan^{-1}\sqrt{r_z}, \tag{C.3}$$

which is equivalent to the equation $v'(w_{\max}) = 0$. The dependency $\sigma(\rho)$ following from this relation is plotted in figure 3(c). In particular, $\rho \approx 1.94$ for $\sigma = 2$ in figure 3(a).

References

[1] Maier S A 2007 *Plasmonics: Fundamentals and Applications* (New York: Springer)

[2] Gramotnev D and Bozhevolnyi S 2010 Plasmonics beyond the diffraction limit *Nature Photon.* **4** 83–91

[3] Lal S, Link S and Halas N 2007 Nano-optics from sensing to waveguiding *Nature Photon.* **1** 641–8

[4] Maier S 2006 Plasmonics: metal nanostructures for subwavelength photonic devices *IEEE J. Sel. Top. Quantum Electron.* **12** 1214–20

[5] Zia R, Schuller J, Chandran A and Brongersma M 2006 Plasmonics: the next chip-scale technology *Mater. Today* **9** 20–7

[6] Davoyan A R, Liu W, Miroshnechenko A E, Shadrivov I V, Kivshar Y S and Bozhevolnyi S I 2011 Mode transformation in waveguiding plasmonic structures *Photon. Nanostruct.* **9** 207

[7] Rukhlenko I D, Premaratne M and Agrawal G P 2011 Nonlinear propagation in silicon-based plasmonic waveguides from the standpoint of applications *Opt. Express* **19** 206–17

[8] Liu J, Zhao H, Zhang Y and Liu S 2009 Resonant cavity based antireflection structures for surface plasmon waveguides *Appl. Phys.* B **98** 797–802

[9] Dionne J A, Sweatlock L A, Atwater H A and Polman A 2006 Plasmon slot waveguides: towards chipscale propagation with subwavelength-scale localization *Phys. Rev.* B **73** 035407

[10] Krenn J and Weeber J 2004 Surface plasmon polaritons in metal stripes and wires *Phil. Trans. R. Soc.* A **362** 739–56

[11] Handapangoda D, Premaratne M, Rukhlenko I D and Jagadish C 2011 Optimal design of composite nanowires for extended reach of surface plasmon-polaritons *Opt. Express* **19** 16058–74

[12] Chen D 2010 Cylindrical hybrid plasmonic waveguide for subwavelength confinement of light *Appl. Opt.* **49** 6868–71

[13] Handapangoda D, Rukhlenko I D, Premaratne M and Jagadish C 2010 Optimization of gain-assisted waveguiding in metal–dielectric nanowires *Opt. Lett.* **35** 4190–2

[14] Oulton R F, Sorger V J, Genov D A, Pile D F P and Zhang X 2008 A hybrid plasmonic waveguide for subwavelength confinement and long-range propagation *Nature Photon.* **2** 496–500

[15] Krishnamurthy V and Klein B 2008 Theoretical investigation of metal cladding for nanowire and cylindrical micropost lasers *IEEE J. Quantum Electron.* **44** 67–74

[16] Jung J, Sondergaard T and Bozhevolnyi S I 2007 Theoretical analysis of square surface plasmon-polariton waveguides for long-range polarization-independent waveguiding *Phys. Rev.* B **76** 035434

[17] Schröter U and Dereux A 2001 Surface plasmon polaritons on metal cylinders with dielectric core *Phys. Rev.* B **64** 125420

[18] Willingham B and Link S 2011 Energy transport in metal nanoparticle chains via sub-radiant plasmon modes *Opt. Express* **19** 6450–61

[19] Udagedara I B, Rukhlenko I D and Premaratne M 2011 Surface plasmon-polariton propagation in piecewise linear chains of composite nanospheres: the role of optical gain and chain layout *Opt. Express* **19** 19973–86
[20] Holmström P, Thylén L and Bratkovsky A 2010 Composite metal/quantum-dot nanoparticle-array waveguides with compensated loss *Appl. Phys. Lett.* **97** 073110
[21] Cui X and Erni D 2008 Enhanced propagation in a plasmonic chain waveguide with nanoshell structures based on low-and high-order mode coupling *J. Opt. Soc. Am.* A **25** 1783–9
[22] Citrin D 2006 Plasmon-polariton transport in metal–nanoparticle chains embedded in a gain medium *Opt. Lett.* **31** 98–100
[23] Citrin D 2004 Coherent excitation transport in metal–nanoparticle chains *Nano Lett.* **4** 1561–5
[24] Pannipitiya A, Rukhlenko I D and Premaratne M 2011 Analytical modeling of resonant cavities for plasmonic-slot-waveguide junctions *IEEE Photonics J.* **3** 220–3
[25] Pannipitiya A, Rukhlenko I D, Premaratne M, Hattori H T and Agrawal G P 2010 Improved transmission model for metal–dielectric–metal plasmonic waveguides with stub structure *Opt. Express* **18** 6191–204
[26] Maier S A 2006 Gain-assisted propagation of electromagnetic energy in subwavelength surface plasmon polariton gap waveguides *Opt. Commun.* **258** 295–9
[27] Veronis G and Fan S 2005 Bends and splitters in metal–dielectric–metal subwavelength plasmonic waveguides *Appl. Phys. Lett.* **87** 131102
[28] Feigenbaum E, Kaminski N and Orenstein M 2009 Negative dispersion: a backward wave or fast light? Nanoplasmonic examples *Opt. Express* **17** 18934–9
[29] Davoyan A R, Shadrivov I V, Bozhevolnyi S I and Kivshar Y S 2010 Backward and forward modes guided by metal–dielectric–metal plasmonic waveguides *J. Nanophoton.* **4** 043509
[30] Prade B, Vinet J Y and Mysyrowicz A 1991 Guided optical waves in planar heterostructures with negative dielectric constant *Phys. Rev.* B **44** 13556–72
[31] Cai W and Shalaev V 2010 *Optical Metamaterials: Fundamentals and Applications* (Berlin: Springer)
[32] Rodriguez-Fortuno F J, Garcia-Meca C, Ortuno R, Marti J and Martinez A 2009 Coaxial plasmonic waveguide array as a negative-index metamaterial *Opt. Lett.* **34** 3325–7
[33] Lezec H J, Dionne J A and Atwater H A 2007 Negative refraction at visible frequencies *Science* **316** 430–2
[34] Shin H and Fan S 2006 All-angle negative refraction for surface plasmon waves using a metal–dielectric–metal structure *Phys. Rev. Lett.* **96** 073907
[35] Landau L D, Lifshitz E M and Pitaevskii L P 1984 *Electrodynamics of Continuous Media* (Oxford: Elsevier, Butterworth-Heinemann)